

Magnetoplasmons in N -layer structures

Jinu Park^{1,*}, Taehun Kim^{1,*}, E. H. Hwang², and Hongki Min^{1†}

¹ Department of Physics and Astronomy, Seoul National University, Seoul 08826, Korea and

² SKKU Advanced Institute of Nanotechnology and Department of Nano Engineering, Sungkyunkwan University, Suwon 16419, Korea

(Dated: February 16, 2026)

We provide a systematic framework to investigate the magnetoplasmons of multilayer two-dimensional electron systems by using the Kac–Murdock–Szegő (KMS) Toeplitz matrix to consider interlayer Coulomb interactions. In the absence of interlayer tunneling, we show that the single-layer magnetoplasmon branch splits into N collective modes—one in-phase mode and $N - 1$ out-of-phase modes—and derive their asymptotic behaviors in the long-wavelength limit, as well as in the limit of large layer separation and strong magnetic fields. When interlayer tunneling is present, we clarify the magnetoplasmon dispersion, both qualitatively and quantitatively, by identifying the magnetoplasmon mode associated with each interband transition, as well as tunneling magnetoplasmons arising from interband transitions with the same Landau level index. Our study presents the hybridization between the modes governed by underlying symmetries, along with an enhanced tunneling magnetoplasmon gap exceeding the associated interband gap. The KMS-based analytic formalism thus provides a comprehensive physical understanding of magnetoplasmons in multilayer structures.

I. INTRODUCTION

Since the realization of two-dimensional (2D) materials such as graphene, transition-metal dichalcogenides, and their heterostructures, multilayer systems have opened up a new area of 2D physics. Recent advances in experimental techniques such as molecular beam epitaxy and exfoliation [1–3] have enabled the fabrication of high-quality layered samples including graphene, quasi-2D materials, and GaAs quantum wells [2, 4–9]. Controlling interlayer interactions through stacking order [10, 11], twist angles [12, 13], and electrostatic gating [14–16] enables a wide range of intriguing electrical phenomena including Coulomb drag effects [14, 17, 18], flat-band superconductivity [19, 20], and interlayer exciton superfluidity [21–23].

Among them, plasmons, which are self-sustained charge density oscillations, in 2D systems have been the focus of active research in recent years due to their influence on the optical and electronic properties of materials [24–31]. In the presence of a magnetic field, they are called magnetoplasmons which are generated by the collective excitations between Landau levels [32–35]. The splitting of plasmon modes due to the cyclotron motion of electrons has been envisioned for promising applications to nanophotonics [36–41]. Furthermore, the possibility of plasmonic excitations to low frequencies has allowed extreme electromagnetic field confinement in multilayer nanostructures, resulting in ultra-strong light-matter coupling [42, 43] and pronounced nonlocal effects [44–46]. This calls for a systematic understanding of magnetoplasmons in multilayer structures.

In this work, we theoretically investigate magnetoplasmon dispersions by incorporating the Kac–Murdock–

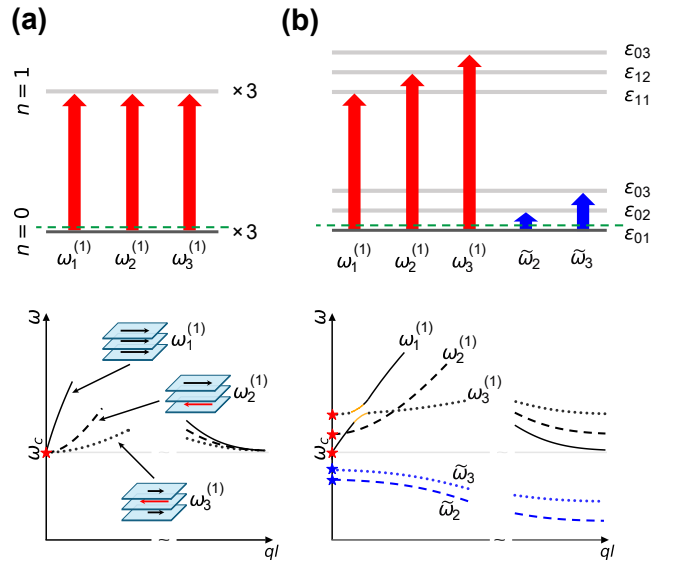


FIG. 1. Schematic illustration of the dominant interband transitions for each mode and the corresponding mode dispersions in a trilayer system filled up to the lowest band: (a) the decoupled-layer limit and (b) the case with finite interlayer tunneling. The green dashed lines denote the Fermi energy, while the black (gray) horizontal lines represent occupied (unoccupied) Landau levels. The red (blue) arrows indicate the dominant transitions in the long-wavelength limit for the magnetoplasmon (tunneling magnetoplasmon) modes. The lower panels show the mode dispersions in the limits of $ql \rightarrow 0$ and $ql \rightarrow \infty$. For a given mode, the same line style is used consistently across the figures. The insets in (a) show the corresponding charge oscillations in the long-wavelength limit. In (b), magnetoplasmon (tunneling magnetoplasmon) modes are depicted by black (blue) lines, and anticrossing behavior between modes is highlighted in yellow.

* These authors contributed equally to this work.

† hmin@snu.ac.kr

Szegő (KMS) Toeplitz matrix into the Landau levels and applying it to systems both with and without interlayer

tunneling. We find that, as in plasmons, the magneto-plasmon dispersion branch in the single-layer case splits into N branches because long-range Coulomb coupling between the layers allows multiple independent collective charge oscillations: one mode in which the charge densities in all layers oscillate in phase, and $N - 1$ modes in which the charge densities oscillate out of phase. We derive the asymptotic behavior of each dispersion in the long-wavelength limit, as well as in the limit of large layer separation and strong magnetic fields. When interlayer tunneling is present, the Landau levels split, and the resulting interband transitions qualitatively modify the magnetoplasmon spectrum. We provide a systematic framework to clarify the spectrum, including the number of modes and their gaps, by identifying the magneto-plasmon mode associated with each interband transition and the hybridization between these modes governed by underlying symmetries. Moreover, interband transitions with the same Landau level index give rise to tunneling magnetoplasmons [47], which acquire an enhanced plasmon gap exceeding the associated interband gap due to the Coulomb interaction. We obtain this correction analytically in the weak Coulomb interaction limit, where the interaction is negligibly small compared to the kinetic energy. Our results for systems filled up to the lowest bands are schematically illustrated in Fig. 1 for the trilayer case.

The paper is organized as follows. In Sec. II, we present the basic formulation of our approach, including the random phase approximation (RPA) and the KMS structure of the Coulomb interaction in the system. The selection rules arising from the system symmetry and interaction structure are also discussed. Section III is devoted to our results for two-dimensional electron gas (2DEG) systems, covering both decoupled cases (Sec. III.A) and coupled cases (Sec. III.B), with particular emphasis on trilayer systems. Finally, the extension to multilayer 2DEG systems with $N > 3$ and to multilayer graphene is discussed in Sec. IV.

II. THEORETICAL BACKGROUND

In this paper, we consider an N -layer system with interlayer separation d under a magnetic field B applied perpendicular to the layers. We retain only nearest-neighbor interlayer tunneling with amplitude t . An eigenstate $|n, \lambda\rangle$ of the system, labeled by a Landau level index n and a subband index $\lambda = 1, \dots, N$, can be written as

$$|n, \lambda\rangle = \sqrt{\frac{2}{N+1}} \sum_{j=1}^N \psi_\lambda^{(j)} |n\rangle_j, \quad (1)$$

where $\psi_\lambda^{(j)} = (-1)^j \sin\left(\frac{j\lambda\pi}{N+1}\right)$ is the subband wave function, and $|n\rangle_j$ denotes the Landau level- n state on the j th layer. The corresponding eigenenergy is $\varepsilon_{n\lambda} = (n + \frac{1}{2}) \hbar\omega_c + \Delta_\lambda$ with $\Delta_\lambda = -2t \cos\left(\frac{\lambda\pi}{N+1}\right)$.

The noninteracting density-density response function of the system at temperature T reads [48, 49]

$$\begin{aligned} \chi_{ij}^{(0)}(\mathbf{q}, \omega) &= \frac{g_s}{2\pi l^2} \sum_{n, n', \lambda, \lambda'} \frac{f(\varepsilon_{n\lambda}) - f(\varepsilon_{n'\lambda'})}{\hbar\omega + \varepsilon_{n\lambda} - \varepsilon_{n'\lambda'} + i0^+} \\ &\times F_{nn'}(\mathbf{q}) P_{ij}^{\lambda\lambda'} \end{aligned} \quad (2)$$

in the layer basis. Here, $g_s = 2$ is the spin degeneracy, $l = \sqrt{\hbar c/(eB)}$ is the magnetic length, $\omega_c = eB/(mc)$ is the cyclotron frequency, ε_F is the Fermi energy, and $f(\varepsilon) = [e^{(\varepsilon - \varepsilon_F)/(k_B T)} + 1]^{-1}$ is the Fermi-Dirac distribution function. The factor

$$P_{ij}^{\lambda\lambda'} = \langle \lambda | P_i | \lambda' \rangle \langle \lambda' | P_j | \lambda \rangle \quad (3)$$

is the wave function overlap factor, where P_i denotes the projector onto the i th layer. The form factor $F_{nn'}(\mathbf{q})$ of a 2DEG is given by [49, 50]

$$F_{n,n'}(\mathbf{q}) = e^{-q^2 l^2/2} \left(\frac{q^2 l^2}{2} \right)^{|n-n'|} \frac{n_<!}{n_>!} \left[L_{n_<}^{|n-n'|} \left(\frac{q^2 l^2}{2} \right) \right]^2, \quad (4)$$

with $n_> = \max(n, n')$, $n_< = \min(n, n')$, and $L_a^b(x)$ denoting the associated Laguerre polynomials.

N -layer magnetoplasmon dispersions are determined by the condition $\det[\epsilon_{ij}(\mathbf{q}, \omega)] = 0$, where ϵ_{ij} is the dielectric matrix, given within the RPA by

$$\epsilon_{ij}(\mathbf{q}, \omega) = \delta_{ij} - \sum_k V_{ik}(q) \chi_{kj}^{(0)}(\mathbf{q}, \omega). \quad (5)$$

$V_{ij}(q) = v(q) e^{-|i-j|qd}$ denotes the Coulomb interaction between the i th layer and j th layer, with $v(q) = 2\pi e^2/(\kappa q)$ and κ the background dielectric constant. For each dispersion $\omega(\mathbf{q})$, the eigenvector of the dielectric matrix with a vanishing eigenvalue describes how the oscillation is distributed among the layers through its coefficients in the layer basis.

The Coulomb matrix $V_{ij}(q)$ can be written in terms of the KMS matrix $A_{ij}(\rho) = \rho^{|i-j|}$ ($0 < \rho < 1$) as $V_{ij}(q) = v(q) A_{ij}(\rho)$ with $\rho = e^{-qd}$, which allows for a tractable analysis of the plasmon dispersions in an N -layer system. The eigenvalues $g_\alpha(e^{-qd})$ and eigenvectors $\mathbf{u}_\alpha(e^{-qd}) = (u_\alpha^{(1)}, \dots, u_\alpha^{(N)})^\top$ ($\alpha = 1, \dots, N$) of $A_{ij}(e^{-qd})$ exhibit well-defined asymptotic forms in both the $qd \rightarrow 0$ and $qd \rightarrow \infty$ limits, as summarized in Table I. For example, for $N = 3$ and $\alpha = 3$ in the $qd \rightarrow 0$ limit, $\mathbf{u}_{\alpha=3}(e^{-qd} \rightarrow 1) = \frac{1}{\sqrt{6}}(1, -2, 1)^\top$, indicating that the first and third layers oscillate in the same direction while the second layer oscillates in the opposite direction with twice their amplitude (see App. A for the explicit expressions of the eigenpairs). In the basis of Coulomb eigenvectors, which diagonalize V_{ij} , the dielectric matrix takes the form

$$\epsilon_{\alpha\beta}(\mathbf{q}, \omega) = \delta_{\alpha\beta} - V_\alpha(q) \chi_{\alpha\beta}^{(0)}(\mathbf{q}, \omega), \quad (6)$$

TABLE I. Asymptotic forms of the eigenvalues $g_\alpha(e^{-qd})$ and the eigenvectors $\mathbf{u}_\alpha(e^{-qd}) = (u_\alpha^{(1)}, \dots, u_\alpha^{(N)})^\top$ of the KMS matrix $A_{ij}(e^{-qd})$. Here $\alpha = 1, \dots, N$ and $k = 1, \dots, N$. The eigenvectors \mathbf{u}_α are presented up to a normalization factor.

Limit	$g_\alpha(e^{-qd})$	$u_\alpha^{(j)}(e^{-qd})$
$qd \rightarrow 0$	$g_1 = N, \quad g_\alpha = \frac{qd}{1 - \cos(\frac{\alpha-1}{N}\pi)} \quad (2 \leq \alpha \leq N)$	$\cos\left[\frac{(2j-1)(\alpha-1)}{2N}\pi\right]$
$qd \rightarrow \infty$	$g_\alpha \simeq 1 + 2e^{-qd} \cos\left(\frac{\alpha\pi}{N+1}\right)$	$\sin\left(\frac{\alpha j\pi}{N+1}\right)$

where $V_\alpha(q) = v(q) g_\alpha(e^{-qd})$. The susceptibility $\chi_{\alpha\beta}^{(0)}$ is obtained from Eq. (2) by replacing $P_{ij}^{\lambda\lambda'}$ in Eq. (3) with

$$P_{\alpha\beta}^{\lambda\lambda'} = \langle \lambda | U_\alpha | \lambda' \rangle \langle \lambda' | U_\beta | \lambda \rangle, \quad (7)$$

where $U_\alpha = \text{diag}[\mathbf{u}_\alpha(e^{-qd})]$.

Coulomb eigenvectors \mathbf{u}_α exhibit symmetry under layer inversion, which provides a selection rule for interband-transition contributions to Coulomb oscillations [51]. Odd-index Coulomb eigenvectors are symmetric under layer inversion about the midplane, whereas even-index eigenvectors are antisymmetric. In a system whose bands are either symmetric or antisymmetric, interband transitions between a symmetric and an antisymmetric band contribute exclusively to antisymmetric Coulomb oscillations, whereas all other transitions contribute to symmetric Coulomb oscillations. In our system, the odd (even) subband index corresponds to a symmetric (antisymmetric) band with respect to layer inversion, and thus band transitions between subband indices of the same (opposite) parity contribute only to Coulomb oscillations of odd (even) index.

In addition to the symmetry constraint, a further selection rule is present in our system. The term $\langle \lambda | U_\alpha | \lambda' \rangle$ is negligible in the long-wavelength limit unless $|\lambda - \lambda'| = \alpha - 1$ or $|\lambda + \lambda' - (N+1)| = N+1 - (\alpha-1)$. For example, the matrix element $\langle \lambda = 1 | U_\beta | \lambda' = \alpha \rangle$ is appreciable only for $\beta = \alpha$ and $\beta = \alpha+2$; both are allowed by the selection rule, but the former is numerically larger in practice. See Sec. III of the Supplemental Material (SM) in Ref. [51] for the explicit derivation. The quantity $P_{\alpha\beta}^{\lambda\lambda'}$ is dominant when both α and β satisfy this condition for given λ and λ' . This rule specifies the Coulomb eigenmodes to which a given interband transition predominantly contributes.

III. RESULTS

A. Decoupled system

When there is no interlayer tunneling and all N layers are filled up to the same filling factor ν , the noninteracting density response function is diagonal in the layer basis, $\chi_{ij}^{(0)} = \delta_{ij} \chi_0$, where χ_0 denotes the noninteracting response function of a single-layer 2DEG. As a result, the Coulomb eigenvectors diagonalize $\epsilon_{\alpha\beta}$, and the magnetoplasmon dispersion branch that emanates from each

$k\omega_c$ ($k = 1, 2, \dots$) in the single-layer case splits into N branches, denoted by $\omega_\alpha^{(k)}$ ($\alpha = 1, \dots, N$) with the associated Coulomb eigenvector \mathbf{u}_α .

In the long-wavelength limit, the dispersion $\omega_\alpha^{(k)}$ is governed solely by interband transitions with gap $k\hbar\omega_c$. Incorporating only these interband transitions, closed-form expressions for the dispersion $\omega_\alpha^{(k)}$ can be obtained as (see App. B for the derivation)

$$[\omega_\alpha^{(k)}(q)]^2 \xrightarrow[qd, ql \rightarrow 0]{} k^2 \omega_c^2 \quad (8)$$

$$+ \frac{k A_k g_s e^2}{\kappa m} \begin{cases} \frac{\sqrt{2N}}{l^3} \left(\frac{q^2 l^2}{2}\right)^{k-1/2}, & \alpha = 1, \\ \frac{2d/l^4}{1 - \cos[\pi(\alpha-1)/N]} \left(\frac{q^2 l^2}{2}\right)^k, & \alpha \neq 1, \end{cases}$$

and in the limit of large layer separation and strong magnetic fields, i.e., $qd, ql \rightarrow \infty$, the magnetoplasmons behave like

$$[\omega_\alpha^{(k)}(q)]^2 \xrightarrow[qd, ql \rightarrow \infty]{} k^2 \omega_c^2 + \left[1 + 2e^{-qd} \cos\left(\frac{\alpha\pi}{N+1}\right) \right] \times \frac{e^{-q^2 l^2/2}}{(\nu + n - 1)!(\nu - 1)!} \frac{k g_s e^2}{\kappa m} \frac{\sqrt{2}}{l^3} \left(\frac{q^2 l^2}{2}\right)^{k+2\nu-5/2}, \quad (9)$$

where $A_k \equiv \sum_{j=j_k}^{\nu-1} \frac{(j+k)!}{j!(k!)^2}$ and $j_k = \max(0, \nu - k)$. Note that the $k = 1$ branches carry the lowest power of q and therefore govern the leading long-wavelength behavior in Eq. (8). The in-phase mode ($\alpha = 1$) within these branches shows a linear dependence on q in the long-wavelength limit, rather than the conventional \sqrt{q} behavior of the non-magnetic mode.

We present numerical results for a decoupled trilayer system in Fig. 2 as an example. The asymptotic forms of $\omega_\alpha^{(k)}$ given by Eq. (8) and Eq. (9) agree with the numerical results. In general, for $k = 1$ the agreement between the numerical results and Eq. (8) is robust regardless of the magnetic-field strength, whereas for $k \neq 1$ the agreement becomes more evident as the magnetic field increases. The reason is that, for each $\omega_\alpha^{(k \neq 1)}$, the range of q over which the transitions with band gap $k\hbar\omega_c$ provide the dominant contribution to the dispersion shrinks as the magnetic field increases. Typically, the parameter $\frac{e^2}{\kappa l} / (\hbar\omega_c)$ controls the range of validity of the asymptotic behavior; thus, the agreement improves at higher magnetic fields or smaller κ .

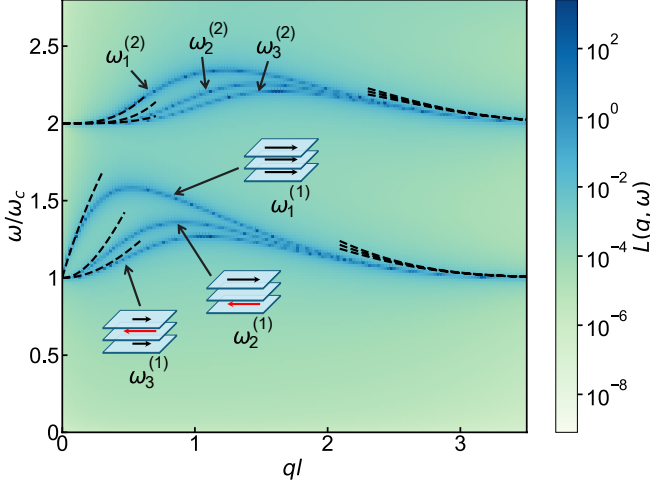


FIG. 2. Loss function plot $L(\mathbf{q}, \omega) = -\text{ImTr}[\epsilon^{-1}(\mathbf{q}, \omega)]$ for a trilayer system in the decoupled limit, compared with the asymptotic forms in Eq. (8) and Eq. (9), which are drawn as black dashed lines. The inset displays Coulomb oscillations for the $\omega_\alpha^{(1)}$ ($\alpha = 1, 2, 3$) modes; note that $\omega_\alpha^{(2)}$ exhibits an identical oscillation pattern. For the calculations, we used parameters typical for a GaAs quantum well: $m = 0.067 m_e$, $\kappa = 10.9$, $d = 100 \text{ \AA}$, and $\hbar\omega_c = 15 \text{ meV}$, with a phenomenological broadening $\eta = 10^{-3} \hbar\omega_c$.

B. Coupled system

Unlike the decoupled case, interlayer tunneling t lifts the Landau level degeneracy by splitting each level into multiple subbands. As a result, the Fermi energy ε_F can lie between the bands sharing the same Landau level index n , resulting in a partially filled Landau level and enabling intersubband transitions within the same Landau level to become allowed. To simplify the band sequence in energy, we primarily focus on the limit $t \ll \hbar\omega_c$, as illustrated in Fig. 1. Note that the qualitative features of our results persist for $t \gtrsim \hbar\omega_c$, as discussed in the Sec. IV.

We first focus on the cases where the system is filled up to the band ε_{01} , so that only the lowest subband $\lambda = 1$ of the $n = 0$ Landau level is fully occupied. The interband transitions between bands with different Landau level indices result in magnetoplasmon dispersions similar to those in the decoupled case. They can be labeled by their gap values as

$$\hbar\omega_\alpha^{(k)}(ql \rightarrow 0) = \Delta_{\alpha 1} + k\hbar\omega_c, \quad (10)$$

with a positive integer k , $\alpha = 1, \dots, N$, and $\Delta_{ij} = \Delta_i - \Delta_j$. The corresponding dominant interband transition in the long-wavelength limit occurs between the band ε_{01} and the band $\varepsilon_{k\alpha}$. As the inversion symmetry is determined by the parity of α , the mode $\omega_\alpha^{(k)}$ follows the parity of α . Thus, we can expect crossing (anticrossing) behavior between modes $\omega_\alpha^{(k)}$ with opposite (same) α parity. Moreover, the transition between ε_{01} and $\varepsilon_{k\alpha}$

predominantly contributes to the Coulomb oscillations associated with \mathbf{u}_α as dictated by the selection rule.

As a specific example, we consider a coupled trilayer system filled up to the state ε_{01} [see Fig. 3(a)]. Three dispersions at and above ω_c correspond to the modes $\omega_\alpha^{(1)}$ ($\alpha = 1, 2, 3$) and show exact agreement with Eq. (10). Moreover, anticrossing behavior is observed between $\omega_1^{(1)}$ and $\omega_3^{(1)}$, while they both cross with $\omega_2^{(1)}$.

The remaining interband transitions between the bands with the same Landau level index give rise to the tunneling magnetoplasmon modes, $\tilde{\omega}_\alpha$ ($\alpha = 2, \dots, N$). Tunneling magnetoplasmon modes acquire an additional gap enhancement relative to the underlying interband gap due to the Coulomb interaction unlike other magnetoplasmon modes $\omega_\alpha^{(k)}$. This property can be checked analytically in the weak Coulomb interaction limit, defined by the condition $(e^2/kl)/t \ll 1$. In this limit, the dominant interband transition contributing to $\tilde{\omega}_\alpha$ occurs between ε_{01} and $\varepsilon_{0\alpha}$ in both the $ql \rightarrow 0$ and $ql \rightarrow \infty$ limits. The values of $\tilde{\omega}_\alpha$ in these limits are given by (see App. C for the explicit derivation)

$$[\hbar\tilde{\omega}_\alpha(ql \rightarrow 0)]^2 = \Delta_{\alpha 1}^2 + (V_\alpha P_{\alpha,\alpha}^{\alpha 1} + V_{\alpha+2} P_{\alpha+2,\alpha+2}^{\alpha 1}) \frac{g_s \Delta_{\alpha 1}}{\pi l^2}, \quad (11a)$$

$$\hbar\tilde{\omega}_\alpha(ql \rightarrow \infty) = \Delta_{\alpha 1}, \quad (11b)$$

where we set $V_\alpha = 0$ and $P_{\alpha,\alpha}^{\alpha 1} = 0$ for $\alpha > N$. Here, $V_\alpha(qd \rightarrow 0)$ is finite because $g_\alpha(e^{-qd})$ has a linear dependence on qd when $\alpha \neq 1$.

It is worth emphasizing that Eq. (11) remains valid for $N = 3$ even when the weak Coulomb interaction limit is not satisfied. In Fig. 3(a), the two dispersions below ω_c correspond to tunneling magnetoplasmons $\tilde{\omega}_\alpha$. Both are well described by Eq. (11), even though the Coulomb interaction is not weak. This agreement originates from the selection rule in the Coulomb eigenbasis, which ensures that each dispersion $\tilde{\omega}_\alpha$ arises from the interband transition between ε_{01} and $\varepsilon_{0\alpha}$. Specifically, the transition between ε_{01} and ε_{03} ($\tilde{\omega}_3$) involves symmetric bands and therefore couples only to odd Coulomb oscillations, whereas the transition between ε_{01} and ε_{02} ($\tilde{\omega}_2$) couples only to an even Coulomb oscillation.

We now consider the case in which higher bands are occupied. When multiple bands are filled, more than one interband transition corresponds to the same plasmon gap. As a result, several magnetoplasmon branches emerge from the same gap, originating from different transitions and subsequently hybridizing and splitting into distinct collective modes. Accordingly, Eq. (10) can be generalized to

$$\hbar\omega_\alpha^{(k)}(ql \rightarrow 0) = \Delta_{\lambda' \lambda} + k\hbar\omega_c, \quad (12)$$

where λ and λ' denote the subband indices of the interband transitions between $\varepsilon_{n\lambda}$ and $\varepsilon_{n'=n+k,\lambda'}$ for a given band filling.

However, the number of such modes is generally non-trivial, since distinct interband transitions may support

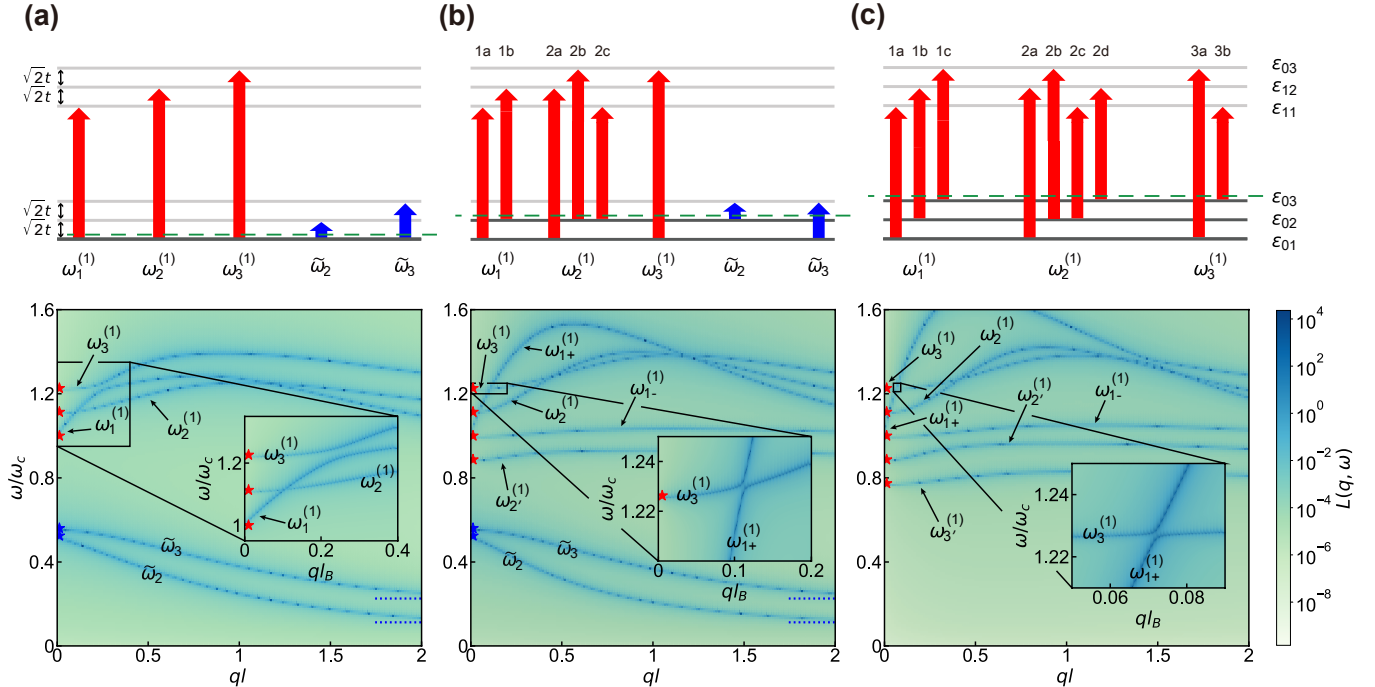


FIG. 3. Schematic illustration of magnetoplasmons associated with each band transition and the loss function plot $L(\mathbf{q}, \omega) = -\text{ImTr}[\epsilon^{-1}(\mathbf{q}, \omega)]$ for a coupled trilayer system filled up to the states (a) ε_{01} , (b) ε_{02} , and (c) ε_{03} . For band transitions indicated by red (blue) arrows, the corresponding magnetoplasmons (tunneling magnetoplasmons) are listed above the arrows. When multiple magnetoplasmons share the same gap, a splitting occurs unless the modes are related by subband-index-reversal symmetry. For example, in (b), $\omega_{1a}^{(1)}$ and $\omega_{1b}^{(1)}$ combine to form $\omega_{1\pm}^{(1)}$, whereas $\omega_{2a}^{(1)}$ and $\omega_{2b}^{(1)}$ are degenerate and form only $\omega_2^{(1)}$. The red and blue stars indicate the magnetoplasmon and tunneling magnetoplasmon gap values evaluated using Eq. (10) for the red stars in (a), Eq. (12) for the red stars in (b) and (c), and Eq. (11a) for the blue stars. The blue dashed lines represent Eq. (11b). The insets in each panel highlight the crossing and anticrossing behaviors between modes; the corresponding regions are indicated by black boxes. The calculations were performed using the same parameters as in Fig. (1), except that $t = 0.8$ meV.

identical Coulomb oscillations. This occurs when two transitions share the same Landau level indices and their subband indices are related by subband-index-reversal symmetry about the central subband, defined by $\lambda \rightarrow N + 1 - \lambda$ and $\lambda' \rightarrow N + 1 - \lambda'$. Specifically, these correspond to the transition between $\varepsilon_{n\lambda}$ and $\varepsilon_{n'\lambda'}$, and that between $\varepsilon_{n,N+1-\lambda}$ and $\varepsilon_{n',N+1-\lambda'}$. These two transitions share the same energy gap due to the relation $\Delta_\lambda = -\Delta_{N+1-\lambda}$, and the fact that they support identical Coulomb oscillations arises from the symmetry properties of $P_{\alpha\beta}^{\lambda\lambda'}$ in Eq. (3), which obeys

$$P_{\alpha\beta}^{\lambda\lambda'} = P_{\alpha\beta}^{(N+1-\lambda)(N+1-\lambda')} = P_{\alpha\beta}^{(N+1-\lambda')(N+1-\lambda)}. \quad (13)$$

The first equality follows from the relation between the subband wave functions, $\psi_\lambda^{(j)} = (-1)^{j+1} \psi_{N+1-\lambda}^{(j)}$, while the second equality reflects the Hermiticity of $P_{\alpha\beta}^{\lambda\lambda'}$, which is real and satisfies $P_{\alpha\beta}^{\lambda\lambda'} = P_{\alpha\beta}^{\lambda'\lambda}$. Since $P_{\alpha\beta}^{\lambda\lambda'}$ determines the dielectric matrix $\epsilon_{\alpha\beta}$, distinct interband transitions sharing the same energy gap and identical $P_{\alpha\beta}^{\lambda\lambda'}$ support the same Coulomb oscillations.

As an example, we first consider the case where a trilayer is filled up to the state ε_{02} [see Fig. 3(b)]. In this ex-

ample, we focus on the case $k = 1$ in Eq. (12). The six interband transitions between $\varepsilon_{0\lambda}$ and $\varepsilon_{1\lambda'}$ can be grouped according to $|\lambda - \lambda'| = 0, 1, 2$, and the corresponding magnetoplasmon modes are labeled as illustrated in the figure. For example, $\omega_{1a}^{(1)}$ corresponds to the magnetoplasmon arising from the transition between ε_{01} and ε_{11} , whereas $\omega_{1b}^{(1)}$ corresponds to the transition between ε_{02} and ε_{12} .

The modes $\omega_{1a}^{(1)}$ and $\omega_{1b}^{(1)}$ share the same gap value $\hbar\omega_c$ and hybridize to form the magnetoplasmon dispersions $\omega_{1\pm}^{(1)}$, which emerge from ω_c . In contrast, the band transitions associated with the magnetoplasmons $\omega_{2a}^{(1)}$ and $\omega_{2b}^{(1)}$ are related by subband-index-reversal symmetry; therefore, no splitting occurs and a unique mode $\omega_2^{(1)}$ emerges from $\omega_c + \sqrt{2}t/\hbar$. The mode $\omega_{2c}^{(1)}$ does not have a transition with the same gap and thus remains as a single branch $\omega_2^{(1)}$ emerging from $\omega_c - \sqrt{2}t/\hbar$, similar to $\omega_3^{(1)}$, which emerges from $\omega_c + 2\sqrt{2}t/\hbar$. As a result, the six transitions give rise to a total of five modes, all of which exhibit gaps consistent with Eq. (12). As in the case where only the lowest band is filled, anticrossing behav-

ior is observed between modes with the same parity, such as $\omega_{1+}^{(1)}$ and $\omega_3^{(1)}$.

Since interband transitions with the same Landau level index n are present in this example, tunneling magnetoplasmons appear. The symmetry rule indicates that the tunneling magnetoplasmons in this system are identical, in the long-wavelength limit, to those in the case where only the lowest band is filled. This equivalence follows from the fact that the band transition between ε_{02} and ε_{03} is mapped onto the transition between ε_{01} and ε_{02} by subband-index-reversal symmetry. As a result, Eq. (11) can be used to describe the tunneling magnetoplasmons shown in Fig. 3(b).

Next, we consider a trilayer filled up to ε_{03} [see Fig. 3(c)]. Nine interband transitions between $\varepsilon_{0\lambda}$ and $\varepsilon_{1\lambda'}$ are available in the system. Grouping the modes as in the previous example, $\omega_{1a}^{(1)}$, $\omega_{1b}^{(1)}$, and $\omega_{1c}^{(1)}$ are the three magnetoplasmons originating from the band transitions across the gap $\hbar\omega_c$. Owing to subband-index-reversal symmetry, $\omega_{1a}^{(1)}$ and $\omega_{1c}^{(1)}$ are identical; these modes hybridize with $\omega_{1b}^{(1)}$, giving rise to $\omega_{1\pm}^{(1)}$. Moreover, $\omega_{2a}^{(1)}$ and $\omega_{2b}^{(1)}$ are identical and together form $\omega_2^{(1)}$, while $\omega_{2c}^{(1)}$ and $\omega_{2d}^{(1)}$ are identical, forming $\omega_2^{(1)}$; both cases come from subband-index-reversal symmetry. In contrast, $\omega_{3a}^{(1)}$ and $\omega_{3b}^{(1)}$ have no transitions with the same gap and therefore give rise to $\omega_3^{(1)}$ and $\omega_{3'}^{(1)}$, respectively. In total, six magnetoplasmons emerge from the nine transitions. All gap positions coincide with those in the previous example except for $\omega_{3'}^{(1)}$, which emerges from $\omega_c - 2\sqrt{2}t/\hbar$, in agreement with Eq. (12). No tunneling magnetoplasmon modes exist in this case, since there is no available band transition between $\varepsilon_{0\lambda}$ and $\varepsilon_{0\lambda'}$. The general ideas illustrated by these examples can be straightforwardly extended to multilayer systems, which will be discussed in the next section.

IV. DISCUSSION AND CONCLUSION

In this section, we discuss the magnetoplasmon dispersions in N -layer 2DEG systems with $N > 3$, as well as those in graphene multilayer systems. In both cases, we observe crossing (anticrossing) behaviors between magnetoplasmon modes with opposite (same) parity, together with the emergence of tunneling magnetoplasmons. Our key results for identifying individual modes in coupled N -layer systems, based on the hybridization between magnetoplasmon modes associated with different band transitions, extend directly to these systems.

We first consider N -layer 2DEG systems with $N > 3$ in the presence of interlayer tunneling. (The description of the decoupled case for general N is given in Sec. III.A.) When the system is filled only up to the lowest band, no qualitative differences arise in the magnetoplasmon modes $\omega_\alpha^{(k)}$ described by Eq. (10). By contrast, additional corrections are generally required for tunneling

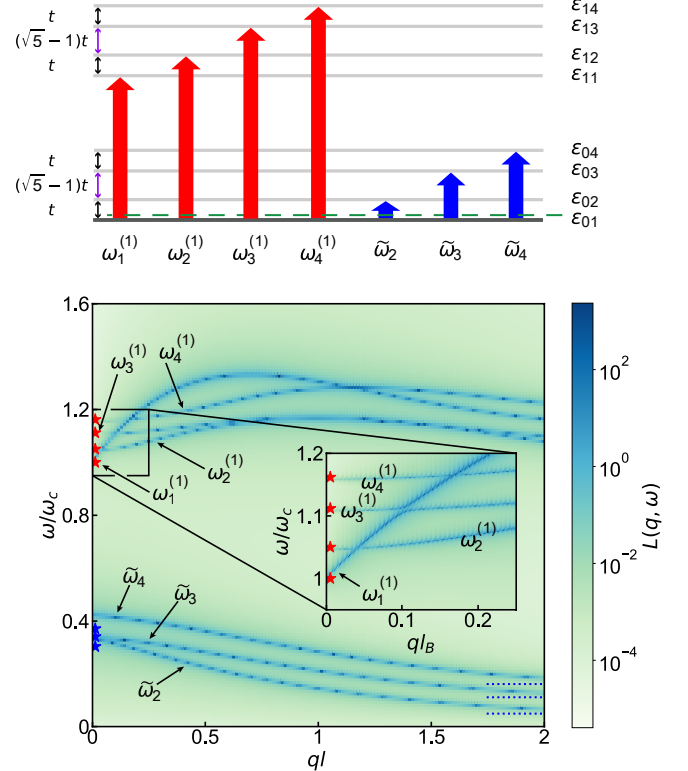


FIG. 4. Schematic illustration of magnetoplasmons associated with each band transition in the weak Coulomb interaction limit, together with the loss function plot $L(\mathbf{q}, \omega) = -\text{Im} \text{Tr}[\epsilon^{-1}(\mathbf{q}, \omega)]$, for a coupled tetralayer system filled up to the state ε_{01} . The same parameters as in Fig. 3(a) are used with $t = 0.5$ meV. Unlike Fig. 3(a), the blue stars obtained from Eq. (11a) deviate from the actual tunneling magnetoplasmon gaps, reflecting additional contributions from interband transitions other than the dominant one in the weak Coulomb interaction limit. By contrast, the red stars obtained from Eq. (10) correctly reproduce the magnetoplasmon gaps.

magnetoplasmons in Eq. (11a), since the assumption of a single dominant interband transition is no longer valid.

In a tetralayer system filled up to the lowest band (see Fig. 4), there are four magnetoplasmon modes $\omega_\alpha^{(k)}$ ($\alpha = 1, \dots, 4$) emerging from each multiple $k\omega_c$ ($k = 1, 2, \dots$). The dominant interband transitions underlying these modes occur between ε_{01} and $\varepsilon_{k\alpha}$, and anticrossing behavior is observed between $\omega_1^{(k)}$ and $\omega_3^{(k)}$, analogous to the trilayer case. For tunneling magnetoplasmons, as in the trilayer case, the selection rule ensures that $\tilde{\omega}_3$ originates from a single interband transition showing excellent agreement with Eq. (11a), while $\tilde{\omega}_2$ and $\tilde{\omega}_4$ are coupled, leading to deviations from Eq. (11a). Nevertheless, the asymptotic behavior described by Eq. (11b) remains valid.

When bands other than the lowest one are filled, additional complexity arises from the unequal spacing be-

tween split bands in the presence of interlayer tunneling. As a result, band transitions rarely share the same energy gap unless they are related by subband-index-reversal symmetry. When degeneracies not protected by the symmetry do occur, hybridization induces a splitting analogous to that observed in trilayer systems. This behavior is most commonly observed in transitions with gaps of $k\hbar\omega_c$, as the gap of transitions between $\varepsilon_{n\lambda}$ and $\varepsilon_{n'=\pm k, \lambda'=\lambda}$ is insensitive to the unequal level spacings. See App. D for tetralayer systems filled up to ε_{02} .

When the interlayer tunneling t becomes comparable to $\hbar\omega_c$ (see the middle panel of Fig. 5), no qualitative differences arise compared to the weak-tunneling regime $t \ll \hbar\omega_c$, except that the ordering of modes in energy can change. As a consequence, crossing (anticrossing) behavior is observed between magnetoplasmon modes $\omega_\alpha^{(k)}$ and tunneling magnetoplasmon modes $\tilde{\omega}_\beta$ with opposite (same) parities of α and β when their dispersions meet. In this regime, Eq. (10) and Eq. (12) remain valid, and Eq. (11a) continues to hold in trilayer systems or in the weak Coulomb interaction limit. Furthermore, essential features observed when bands other than the lowest one are filled, such as splittings arising from the absence of subband-index-reversal symmetry, persist irrespective of the relative magnitude of t and $\hbar\omega_c$.

In the limit $t \gg \hbar\omega_c$, the dispersion relations in the $B \rightarrow 0$ limit are recovered, as the spectral weight distributed among a number of magnetoplasmon modes collectively reconstructs features of non-magnetic systems—specifically, plasmon dispersions and the electron-hole continuum. Moreover, when the density is confined to the lowest parabolic band of non-magnetic N -layer systems, Eq. (11) describes the gap value of out-of-phase plasmon modes [51] in the $B \rightarrow 0$ limit, while one in-phase mode is formed by the combination of numerous $\omega_1^{(k)}$. This confirms that tunneling magnetoplasmons are longitudinal modes and originate from the bulk of the N -layer system. See the bottom panel of Fig. 5 for numerical results in trilayer 2DEG systems with $t/(\hbar\omega_c) = 10$ in the regime where the total electron density is confined to the lowest parabolic band.

The theoretical approach developed here is generalizable beyond the trilayer and tetralayer examples discussed. The symmetry-based mode classification offers a robust tool for analyzing complex spectral features in systems with an arbitrary number of layers N . Furthermore, we emphasize that the framework can be straightforwardly extended to other multilayer platforms, such as graphene, where unequal Landau level spacing introduces additional complexity. In the case of N -layer graphene, the major difference stems from the unequal Landau level spacing, resulting in a complex spectrum of magnetoplasmons compared to that of a 2DEG. However, we observe that our key results can be applied straightforwardly. See App. E for the numerical results of N -layer graphene systems.

In summary, we have established a systematic theoretical framework for analyzing magnetoplasmons in N -

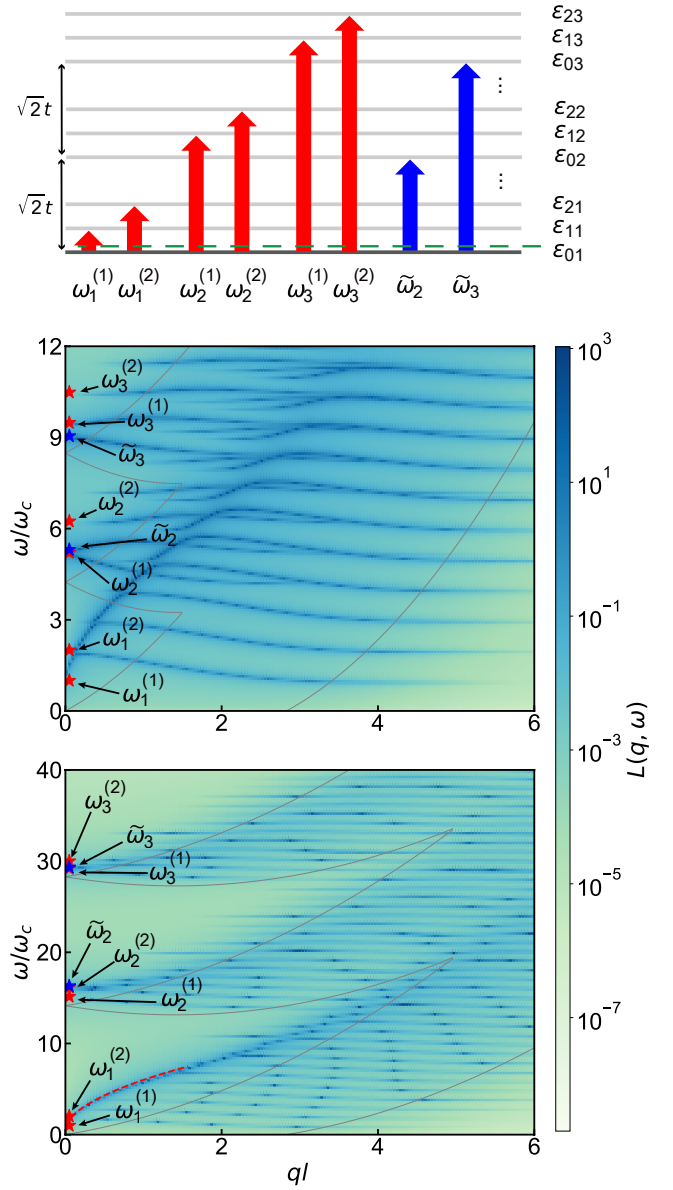


FIG. 5. The top panel shows a schematic illustration of magnetoplasmons associated with each band transition for a trilayer system filled up to the state ε_{01} in the limit $t \gg \hbar\omega_c$. The middle and bottom panels display the loss function plot $L(\mathbf{q}, \omega) = -\text{Im} \text{Tr}[\epsilon^{-1}(\mathbf{q}, \omega)]$ calculated for $t/(\hbar\omega_c) = 3$ and $t/(\hbar\omega_c) = 10$, respectively, with fixed $t = 0.5$ meV. As in Fig. 3, the red and blue stars correspond to results from Eq. (10) and Eq. (11a), respectively. The gray lines indicate the boundaries of the electron-hole continuum in a coupled trilayer 2DEG system at zero magnetic field, corresponding to total electron densities of $n_{\text{tot}} = 2.33 \times 10^9 \text{ cm}^{-2}$ (middle panel) and $n_{\text{tot}} = 0.70 \times 10^9 \text{ cm}^{-2}$ (bottom panel).

layer 2DEG systems. Our analysis clarifies how the magnetoplasmon spectra are governed by the interplay between the Coulomb interaction and interlayer tunneling. In the decoupled limit, we showed that the single-layer

modes split into N branches, whose asymptotic behaviors are obtained in the long-wavelength limit, as well as in the limit of large layer separation and strong magnetic fields. In the presence of interlayer tunneling, the lifting of Landau level degeneracy allows for multiple interband transitions. We demonstrated that the spectral structure is determined by the hybridization between magnetoplasmon modes associated with these distinct transitions. This hybridization is strictly governed by symmetry constraints—specifically parity and subband-index-reversal symmetry—which lead to distinct crossing or anticrossing behaviors. Furthermore, we identified the origin of tunneling magnetoplasmons arising from intra-Landau-level transitions and provided an analytical description of their gap enhancement in the weak interaction limit. We point out that our approach can be generalized to systems with an arbitrary number of layers N as well as other multilayer platforms including graphene. We hope that our detailed quantitative investigation (comprising both numerical and analytical results) of the magnetoplasmons and loss functions will motivate experimental studies (e.g., involving inelastic light scattering and far-infrared frequency-domain spectroscopy) on collective dynamics in multilayer quantum Hall systems.

ACKNOWLEDGMENTS

The work at SNU was supported by the National Research Foundation of Korea (NRF) grants funded by the Korean government (MSIT) (Grant No. RS-2023-NR076715), the Creative-Pioneering Researchers Program through Seoul National University (SNU), and the Center for Theoretical Physics. EHH acknowledges support from the National Research Foundation of Korea (NRF) (Grant No. RS-2021-NR058646).

Appendix A: Eigenvalues and eigenvectors of KMS matrix

In this section, we review the properties of the eigenvalues and eigenvectors of the KMS matrix defined by $A_{ij} = \rho^{|i-j|}$ for $0 < \rho < 1$ and $1 \leq i, j \leq N$:

$$A = \begin{pmatrix} 1 & \rho & \rho^2 & \cdots & \rho^{N-2} & \rho^{N-1} \\ \rho & 1 & \rho & \cdots & \rho^{N-3} & \rho^{N-2} \\ \rho^2 & \rho & 1 & \cdots & \rho^{N-4} & \rho^{N-3} \\ \vdots & \vdots & \vdots & \ddots & \vdots & \vdots \\ \rho^{N-2} & \rho^{N-3} & \rho^{N-4} & \cdots & 1 & \rho \\ \rho^{N-1} & \rho^{N-2} & \rho^{N-3} & \cdots & \rho & 1 \end{pmatrix}. \quad (\text{A1})$$

The analysis presented below follows Ref. [51] and its SM. Here, we omit the explicit derivation and instead focus on extracting the analytical properties relevant to the regime of interest. The eigenvalues $g_\alpha(\rho)$ and the

eigenvectors $\mathbf{u}_\alpha = (u_\alpha^{(1)}, u_\alpha^{(2)}, \dots, u_\alpha^{(N)})^\top$ are given by [51–56]

$$g_\alpha(\rho) = \frac{1 - \rho^2}{1 - 2\rho \cos(\theta_\alpha) + \rho^2}, \quad (\text{A2})$$

$$u_\alpha^{(j)}(\rho) = \sin \left[\frac{\alpha}{N+1} j\pi + \left(\frac{1}{2} - \frac{j}{N+1} \right) \eta_\alpha(\rho) \right]. \quad (\text{A3})$$

where

$$\eta_\alpha(\rho) = 2 \arctan \left[\frac{\rho \sin(\theta_\alpha)}{1 - \cos(\theta_\alpha)} \right]$$

and θ_α ($\frac{\alpha-1}{N}\pi < \theta_\alpha < \frac{\alpha}{N}\pi$) is the unique solution to the equation

$$(N+1)\theta_\alpha + \eta_\alpha(\rho) = \alpha\pi. \quad (\text{A4})$$

In the limit $\rho \rightarrow 1$, we find $\eta_\alpha(\rho) \rightarrow \pi - \theta_\alpha$ from the relation $\frac{\sin(x)}{1-\cos(x)} = \cot(x/2)$, yielding $\theta_\alpha \rightarrow \frac{\alpha-1}{N}\pi$. The corresponding eigenpairs become

$$g_\alpha(\rho \rightarrow 1) = \begin{cases} N, & \alpha = 1, \\ \frac{1 - \rho}{1 - \cos\left(\frac{\alpha-1}{N}\pi\right)}, & 2 \leq \alpha \leq N, \end{cases} \quad (\text{A5})$$

$$u_\alpha^{(j)}(\rho \rightarrow 1) = \cos \left[\frac{(2j-1)(\alpha-1)}{2N} \pi \right]. \quad (\text{A6})$$

In the limit $\rho \rightarrow 0$, we have $\eta_\alpha(\rho) \rightarrow 0$ and $\theta_\alpha \rightarrow \frac{\alpha\pi}{N+1}$, where the eigenpairs take the form

$$g_\alpha(\rho \rightarrow 0) = 1 + 2\rho \cos \left(\frac{\alpha\pi}{N+1} \right) + \mathcal{O}(\rho^2), \quad (\text{A7})$$

$$u_\alpha^{(j)}(\rho \rightarrow 0) = \sin \left(\frac{\alpha j \pi}{N+1} \right) + \mathcal{O}(\rho). \quad (\text{A8})$$

By identifying $\rho = e^{-qd}$, the $\rho \rightarrow 1$ and $\rho \rightarrow 0$ limits correspond to the $qd \rightarrow 0$ and $qd \rightarrow \infty$ regimes respectively, and the resulting asymptotic forms for $g_\alpha(e^{-qd})$ and $u_\alpha^{(j)}(e^{-qd})$ are summarized in Table I.

Appendix B: Magnetoplasmon dispersions in single-layer and decoupled N -layer 2DEG systems

At $T = 0$, the noninteracting density-density response function of a single-layer 2DEG at an integer filling factor ν in a perpendicular magnetic field is given by [49]

$$\chi_{2D}^{(0)}(\mathbf{q}, \omega) = N_0 \sum_{k=0}^{\infty} \bar{\chi}_k^{(0)}(\bar{q}, \bar{\omega}), \quad (\text{B1})$$

where $\bar{q} \equiv \frac{q^2 l^2}{2}$, $\bar{\omega} \equiv \frac{\omega^+}{\omega_c}$, $\omega^+ \equiv \omega + i0^+$ and $N_0 \equiv \frac{g_s}{2\pi l^2 \hbar \omega_c} = \frac{g_s m}{2\pi \hbar^2}$ is the zero-field density of states at the Fermi energy with $g_s = 2$ being the spin degeneracy. The parameters $l = \sqrt{\hbar c/(eB)}$ and $\omega_c = eB/(mc)$ denote

the magnetic length and the cyclotron frequency, respectively. The dimensionless function $\bar{\chi}_k^{(0)}(\bar{q}, \bar{\omega})$ is defined as

$$\bar{\chi}_k^{(0)}(\bar{q}, \bar{\omega}) = \frac{2k}{\bar{\omega}^2 - k^2} \sum_{j=j_k}^{\nu-1} \bar{F}_{j+k, k}(\bar{q}), \quad (\text{B2})$$

where $j_k \equiv \max(0, \nu - k)$ and

$$\bar{F}_{n, n'}(\bar{q}) = e^{-\bar{q}} \bar{q}^{|n-n'|} \frac{n_<!}{n_>!} \left[L_{n_<}^{|n-n'|}(\bar{q}) \right]^2 \quad (\text{B3})$$

is the form factor defined in Eq. (4), where $n_> = \max(n, n')$ and $n_< = \min(n, n')$. The associated Laguerre polynomials $L_a^b(x)$ satisfy the asymptotic forms:

$$L_j^k(x \rightarrow 0) = \binom{j+k}{j}, \quad L_j^k(x \rightarrow \infty) \sim (-1)^j \frac{x^j}{j!}.$$

Substituting these forms into Eq. (B1), we obtain the asymptotic behavior for small and large \bar{q} :

$$\bar{\chi}_k^{(0)}(\bar{q}, \bar{\omega}) \rightarrow \begin{cases} A_k \bar{q}^k \frac{2k}{\bar{\omega}^2 - k^2}, & (\bar{q} \rightarrow 0) \\ \frac{e^{-\bar{q}} \bar{q}^{k+2\nu-2}}{(\nu+k-1)!(\nu-1)!} \frac{2k}{\bar{\omega}^2 - k^2}, & (\bar{q} \rightarrow \infty) \end{cases} \quad (\text{B4})$$

where $A_k \equiv \sum_{j=j_k}^{\nu-1} \frac{(j+k)!}{j!(k!)^2}$.

The plasmon dispersions are determined within the random phase approximation (RPA) by solving $\epsilon_{\text{RPA}} = 0$, where

$$\begin{aligned} \epsilon_{\text{RPA}}(\mathbf{q}, \omega) &= 1 - v(q) \chi_{2\text{D}}^{(0)}(\mathbf{q}, \omega) \\ &= 1 - \frac{g_s m e^2 l}{\kappa \hbar^2} \frac{1}{\sqrt{2\bar{q}}} \sum_{k=0}^{\infty} \bar{\chi}_k^{(0)}(\bar{q}, \bar{\omega}) \end{aligned} \quad (\text{B5})$$

with $v(q) = 2\pi e^2/(\kappa q)$ the Coulomb potential and κ the dielectric constant. Near the k th cyclotron harmonic ($\omega \simeq k\omega_c$), the response function $\chi_{2\text{D}}^{(0)}$ is dominated by the k th term $N_0 \bar{\chi}_k^{(0)}$ as the denominator $\bar{\omega}^2 - k^2$ approaches zero. Accordingly, the dispersion analysis can be simplified by retaining only the $\bar{\chi}_k^{(0)}$ term in Eq. (B5). This approximation is valid in both the $\bar{q} \rightarrow 0$ and $\bar{q} \rightarrow \infty$ limits, and its validity range broadens as the ratio $(m e^2 l)/(\kappa \hbar^2) = (e^2/\kappa l)/(\hbar \omega_c)$ decreases [49]. In this regime, the dimensionless asymptotics for $\bar{\omega}(\bar{q})$ are given by:

$$\bar{\omega}^2 - k^2 \xrightarrow{\bar{q} \rightarrow 0} \sqrt{2} k A_k \frac{g_s m e^2 l}{\kappa \hbar^2} \bar{q}^{k-\frac{1}{2}}, \quad (\text{B6})$$

$$\bar{\omega}^2 - k^2 \xrightarrow{\bar{q} \rightarrow \infty} \sqrt{2} k \frac{g_s m e^2 l}{\kappa \hbar^2} \frac{e^{-\bar{q}} \bar{q}^{k+2\nu-\frac{5}{2}}}{(\nu+k-1)!(\nu-1)!}. \quad (\text{B7})$$

Restoring the units yields the following dispersion relations:

$$[\omega^{(k)}(q)]^2 \xrightarrow{q \rightarrow 0} k^2 \omega_c^2 + \frac{\sqrt{2} k A_k g_s e^2}{\kappa m l^3} \left(\frac{q^2 l^2}{2} \right)^{k-1/2}, \quad (\text{B8})$$

$$\begin{aligned} [\omega^{(k)}(q)]^2 &\xrightarrow{q \rightarrow \infty} k^2 \omega_c^2 + \frac{\sqrt{2} k g_s e^2}{\kappa m l^3} \\ &\quad \times \frac{e^{-q^2 l^2/2}}{(\nu+k-1)!(\nu-1)!} \left(\frac{q^2 l^2}{2} \right)^{k+2\nu-5/2}, \end{aligned} \quad (\text{B9})$$

where $\omega^{(k)}$ denotes the magnetoplasmon mode emerging from $k\omega_c$.

The extension to decoupled N -layer systems is straightforward. In the basis of Coulomb eigenvectors, the RPA dielectric tensor is diagonal, $\epsilon_{\alpha\beta}(\mathbf{q}, \omega) = \epsilon_{\alpha}(\mathbf{q}, \omega) \delta_{\alpha\beta}$, with

$$\epsilon_{\alpha}(\mathbf{q}, \omega) = 1 - g_{\alpha}(e^{-qd}) v(q) \chi_{2\text{D}}^{(0)}. \quad (\text{B10})$$

The single-layer magnetoplasmon mode $\omega^{(k)}$ splits into N branches $\omega_{\alpha}^{(k)}$ in the N -layer case. The asymptotics of these modes follow the same functional forms as in Eq. (8) and Eq. (9), obtained by retaining only the contribution from $\bar{\chi}_k^{(0)}$ in $\chi_{2\text{D}}^{(0)}$ when solving the dispersion relation $\epsilon_{\alpha}(\mathbf{q}, \omega) = 0$ and employing the limiting forms of g_{α} (see App. A).

Appendix C: Tunneling magnetoplasmon dispersions in N -layer 2DEG systems filled up to the lowest band

In this section, we derive Eq. (11) in the regime where the interlayer tunneling t satisfies the weak Coulomb interaction limit, defined by the condition $(e^2/\kappa l)/t \ll 1$. To briefly outline the derivation, we first demonstrate that considering only intra-Landau-level transitions in Eq. (2) is sufficient to determine the gap of the tunneling magnetoplasmon modes. This step also accounts for the absence of any additional gap enhancement relative to the underlying interband gap in the magnetoplasmon modes $\omega_{\alpha}^{(k)}$, as stated in Eq. (10) and Eq. (12). We then derive Eq. (11) by considering only a specific interband transition, which is valid in the weak Coulomb interaction regime owing to the small gap enhancement.

Analogous to Eq. (B1), the dimensionless density-density response function for an N -layer 2DEG at $T = 0$ in the Coulomb eigenbasis, obtained by replacing the indices ij in Eq. (2) with $\alpha\beta$, is given by

$$\chi_{\alpha\beta}^{(0)}(\mathbf{q}, \omega) = N_0 \sum_{\substack{\varepsilon_{n\lambda} > \varepsilon_F \\ \varepsilon_{n'\lambda'} < \varepsilon_F}} \bar{\chi}_{n\lambda; n'\lambda'}^{(0)}(\bar{q}, \bar{\omega}), \quad (\text{C1})$$

where $\varepsilon_{n\lambda} = (n + \frac{1}{2})\hbar\omega_c + \Delta_{\lambda}$ is the energy associated with Landau level index n and subband index $\lambda = 1, \dots, N$.

$\Delta_\lambda = -2t \cos\left(\frac{\lambda\pi}{N+1}\right)$ denotes the subband splitting due to interlayer tunneling t . The summation is taken over all n, n', λ , and λ' satisfying $\varepsilon_{n\lambda} > \varepsilon_F$ and $\varepsilon_{n'\lambda'} < \varepsilon_F$. The dimensionless function $\bar{\chi}_{n\lambda;n'\lambda'}^{\alpha\beta}$ is defined as

$$\bar{\chi}_{n\lambda;n'\lambda'}^{\alpha\beta}(\bar{q}, \bar{\omega}) = \frac{2[(n - n') + \bar{\Delta}_{\lambda\lambda'}]}{\bar{\omega}^2 - [(n - n') + \bar{\Delta}_{\lambda\lambda'}]^2} \bar{F}_{n,n'}(\bar{q}) P_{\lambda\lambda'}^{\alpha\beta}. \quad (\text{C2})$$

where $\bar{F}_{n,n'}(\bar{q})$ is the form factor defined in Eq. (B3) and $P_{\alpha\beta}^{\lambda\lambda'} = \langle \lambda | U_\alpha | \lambda' \rangle \langle \lambda' | U_\beta | \lambda \rangle$ is the overlap factor defined in Eq. (7).

The determination of the dispersion relations by solving $\det[\epsilon_{\alpha\beta}(\mathbf{q}, \omega)] = 0$ is more intricate than the analysis presented in App. B. The dielectric matrix is given by

$$\begin{aligned} \epsilon_{\alpha\beta}(\mathbf{q}, \omega) &= \delta_{\alpha\beta} - g_\alpha(e^{-qd}) v(q) \chi_{\alpha\beta}^{(0)}(\mathbf{q}, \omega) \\ &= \delta_{\alpha\beta} - \frac{gme^2 l}{\kappa\hbar^2} \frac{g_\alpha(e^{-qd})}{\sqrt{2\bar{q}}} \sum_{\substack{\varepsilon_{n\lambda} > \varepsilon_F \\ \varepsilon_{n'\lambda'} < \varepsilon_F}} \bar{\chi}_{n\lambda;n'\lambda'}^{\alpha\beta}(\bar{q}, \bar{\omega}) \end{aligned} \quad (\text{C3})$$

in agreement with Eq. (6). Notably, in the limit $\bar{q} \rightarrow 0$, the form factor $\bar{F}_{n,n'}(\bar{q})$ vanishes for $n \neq n'$ due to the $\bar{q}^{|n-n'|}$ factor, which facilitates a tractable analysis of the gap values for each mode. Specifically, in the limit $\bar{q} \rightarrow 0$, $g_\alpha(e^{-qd})$ scales as $qd \sim \sqrt{\bar{q}}$ for $\alpha \neq 1$ and remains constant for $\alpha = 1$ (see Table I). In either case, $\frac{g_\alpha(e^{-qd})}{\sqrt{\bar{q}}} \bar{\chi}_{n\lambda;n'\neq n,\lambda'}^{\alpha\beta}$ vanishes unless the denominator $\bar{\omega}^2 - [(n - n') + \bar{\Delta}_{\lambda\lambda'}]^2$ approaches zero. In contrast, the terms with $n' = n$ can yield a finite contribution to the total response function.

To determine the solutions of $\det(\epsilon_{\alpha\beta}) = 0$ apart from $[\bar{\omega}(\bar{q} \rightarrow 0)]^2 = [(n - n') + \bar{\Delta}_{\lambda\lambda'}]^2$, it is sufficient to consider only the contribution from $\bar{\chi}_{n\lambda;n'=n,\lambda'}^{\alpha\beta}$ in Eq. (C3). Physically, this corresponds to transitions between bands with the same Landau level index, giving rise to tunneling magnetoplasmon modes. On the other hand, magnetoplasmons emerge from the solutions $[\bar{\omega}(\bar{q} \rightarrow 0)]^2 = [(n - n') + \bar{\Delta}_{\lambda\lambda'}]^2$, analogous to the analysis in App. B. No additional finite Coulomb correction occurs relative to the interband gap, as stated in Eq. (10) and Eq. (12).

When the system is filled up to the lowest band ε_{01} , restricting the summation to intra-Landau-level transitions allows Eq. (C1) to be simplified as

$$\chi_{\alpha\beta}^{(0)}(ql \rightarrow 0, \omega) \approx \sum_{\lambda=2}^N P_{\alpha\beta}^{\lambda 1} \frac{g}{2\pi l^2} \frac{2\Delta_{\lambda 1}}{\hbar^2 \omega^2 - \Delta_{\lambda 1}^2}, \quad (\text{C4})$$

which is formally equivalent to the situation discussed in Sec. IV of the SM in Ref. [51]. It is worth emphasizing that the key results of Sec. III of the SM in Ref. [51] remain valid in our system owing to the identical structure of the overlap factor $P_{\alpha\beta}^{\lambda\lambda'}$, which is denoted as $F_{\alpha\beta}^{\lambda\lambda'}$ in the cited work.

The final step of the derivation consists of retaining only the term proportional to $1/(\hbar^2 \omega^2 - \Delta_{\alpha 1}^2)$, which yields Eq. (11a) following Eq. (S23) in the cited work. This procedure is justified under the condition $(e^2/\kappa l)/t \ll 1$, since in this regime, the Coulomb correction term in Eq. (11a)—given explicitly as

$$(V_\alpha P_{\alpha,\alpha}^{\alpha 1} + V_{\alpha+2} P_{\alpha+2,\alpha+2}^{\alpha 1}) \frac{g\Delta_{\alpha 1}}{\pi l^2} \sim \frac{e^2}{\kappa l t}$$

—becomes negligible. Consequently, the term containing $1/(\hbar^2 \omega^2 - \Delta_{\alpha 1}^2)$ dominates Eq. (C4), justifying the single-term consideration.

In the limit $\bar{q} \rightarrow \infty$, the form factor $\bar{F}_{n,n'}(\bar{q})$ vanishes irrespective of the values of n and n' ; thus, Eq. (11b) remains valid by arguments analogous to those for Eq. (10) and Eq. (12).

Appendix D: Magnetoplasmons in a tetralayer 2DEG system filled up to ε_{02}

In this section, we consider a tetralayer 2DEG system filled up to ε_{02} (see Fig. 6). The eight interband transitions between $\varepsilon_{0\lambda}$ and $\varepsilon_{1\lambda'}$ and the corresponding magnetoplasmon modes can be grouped in the same manner as the example illustrated in Fig. 3(b). The hybridization rules, which are governed by parity and subband-index-reversal symmetries, remain equally valid here. For example, $\omega_{1a}^{(1)}$ and $\omega_{1b}^{(1)}$ hybridize to form $\omega_{1\pm}^{(1)}$. The modes $\omega_{3a}^{(1)}$ and $\omega_{3b}^{(1)}$ are related by subband-index-reversal symmetry; therefore, no splitting occurs and a single mode $\omega_3^{(1)}$ emerges at $\omega_c + \sqrt{5}t/\hbar$. The band transitions associated with $\omega_{2a}^{(1)}$, $\omega_{2b}^{(1)}$, $\omega_{2c}^{(1)}$, and $\omega_4^{(1)}$ all possess distinct underlying band gaps, and thus each forms a separate mode. As a result, the eight transitions give rise to a total of seven modes, all of which exhibit gaps consistent with Eq. (12).

Similarly to the tetralayer case filled up to the lowest band (see Fig. 4), the tunneling magnetoplasmon modes can exhibit deviations from Eq. (11) due to the coupling between plasmon modes. Thus, we need to consider a matrix form of $\chi_{\alpha\beta}^{(0)}$, which takes the form

$$\chi_{\alpha\beta}^{(0)}(ql \rightarrow 0, \omega) \approx \sum_{\lambda=3}^4 \sum_{\lambda'=1}^2 P_{\alpha\beta}^{\lambda\lambda'} \frac{g}{2\pi l^2} \frac{2\Delta_{\lambda\lambda'}}{\hbar^2 \omega^2 - \Delta_{\lambda\lambda'}^2}, \quad (\text{D1})$$

where only intra-Landau-level transitions contribute to $\chi_{\alpha\beta}^{(0)}$. Consequently, the tunneling magnetoplasmon modes are determined by solving the condition $\det(\epsilon_{\alpha\beta}) = 0$, incorporating this explicit matrix form of $\chi_{\alpha\beta}^{(0)}$.

The selection rule inherent to the Coulomb eigenbasis simplifies the dispersion analysis. Analogous to the case of $\omega_\alpha^{(k)}$, there are four interband transitions between $\varepsilon_{0\lambda}$ and $\varepsilon_{0\lambda'}$, and the corresponding tunneling magnetoplasmon modes $\tilde{\omega}_\alpha$ can be labeled in a similar manner.

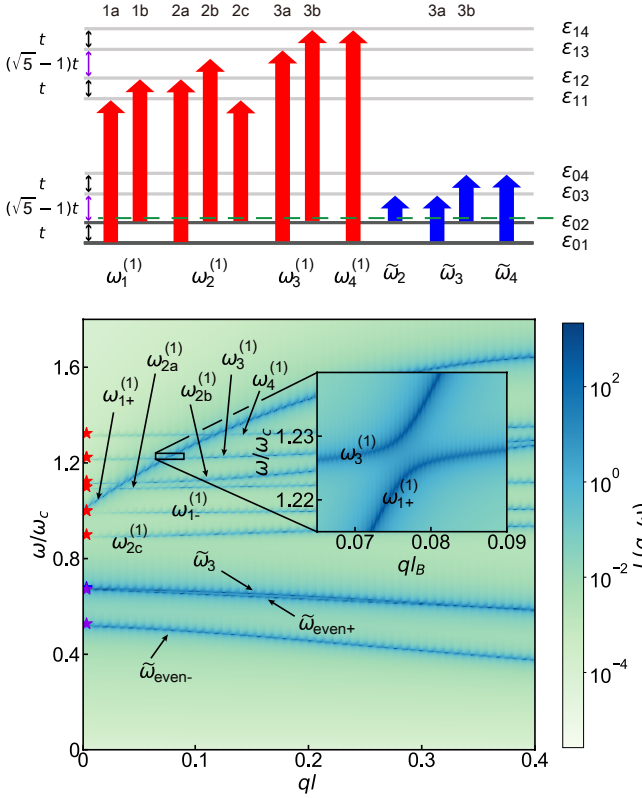


FIG. 6. Schematic illustration of magnetoplasmons associated with each band transition in the weak Coulomb interaction limit, together with the loss function plot $L(\mathbf{q}, \omega) = -\text{Im} \text{Tr}[\epsilon^{-1}(\mathbf{q}, \omega)]$, for a coupled tetralayer system filled up to the state ϵ_{02} . The same parameters as in Fig. 3(a) are used with $\hbar\omega_c = 5 \text{ meV}$ and $t = 0.5 \text{ meV}$. The classification between tunneling magnetoplasmon modes is possible owing to the blue star obtained from Eq. (D2) and the purple stars obtained from Eq. (D3). As in Fig. 4, the red stars obtained from Eq. (12) correctly reproduce the magnetoplasmon gaps.

$\tilde{\omega}_{3a}$ and $\tilde{\omega}_{3b}$ do not couple to either $\tilde{\omega}_2$ or $\tilde{\omega}_4$ owing to their opposite parity. Moreover, since $\tilde{\omega}_{3a}$ and $\tilde{\omega}_{3b}$ are related by subband-index-reversal symmetry, they do not split into two modes but instead form a single mode $\tilde{\omega}_3$ determined by

$$[\hbar\tilde{\omega}_3(ql \rightarrow 0)]^2 = \Delta_{31}^2 + 2V_3P_{3,3}^{31} \frac{g\Delta_{31}}{\pi l^2}, \quad (\text{D2})$$

where the degeneracy of the two modes leads to a factor of two relative to Eq. (10).

The remaining two modes $\tilde{\omega}_2$ and $\tilde{\omega}_4$ hybridize to form $\tilde{\omega}_{\text{even}\pm}$, determined by the condition

$$\det[\epsilon_{\alpha\beta}(q \rightarrow 0, \omega)] \rightarrow [1 - V_2\chi_{22}^{(0)}] [1 - V_4\chi_{44}^{(0)}] - V_2V_4 [\chi_{24}^{(0)}]^2 = 0, \quad (\text{D3})$$

where

$$\chi_{\alpha\beta}^{(0)} \rightarrow \frac{g}{2\pi l^2} \left(P_{\alpha\beta}^{32} \frac{2\Delta_{32}}{\hbar^2\omega^2 - \Delta_{32}^2} + P_{\alpha\beta}^{41} \frac{2\Delta_{41}}{\hbar^2\omega^2 - \Delta_{41}^2} \right)$$

accounts only for the contributions from the band transitions associated with $\tilde{\omega}_2$ and $\tilde{\omega}_4$ in Eq. (D1). This expression yields a quadratic equation in ω^2 that admits analytical solutions $\tilde{\omega}_{\text{even}\pm}$, as illustrated by the purple stars in Fig. 6.

Appendix E: Magnetoplasmons in N -layer graphene systems

In this section, we investigate the magnetoplasmon dispersions in N -layer graphene systems. Unlike conventional 2DEGs, graphene exhibits unequally spaced Landau levels with an energy spectrum given by $\epsilon_n = \text{sgn}(n) \frac{\hbar v_F}{l} \sqrt{2|n|}$, where v_F is the Fermi velocity, $l = \sqrt{\hbar c/(eB)}$ is the magnetic length, and the integer n represents an electron-like ($n > 0$) or hole-like ($n < 0$) Landau level index. Moreover, a single Landau level exists for the case $n = 0$ with $\epsilon_0 = 0$. The bare susceptibility in single-layer graphene required for Eq. (B10) was calculated using the graphene form factor in Ref. [50]. Despite the complexity arising from this unequal Landau

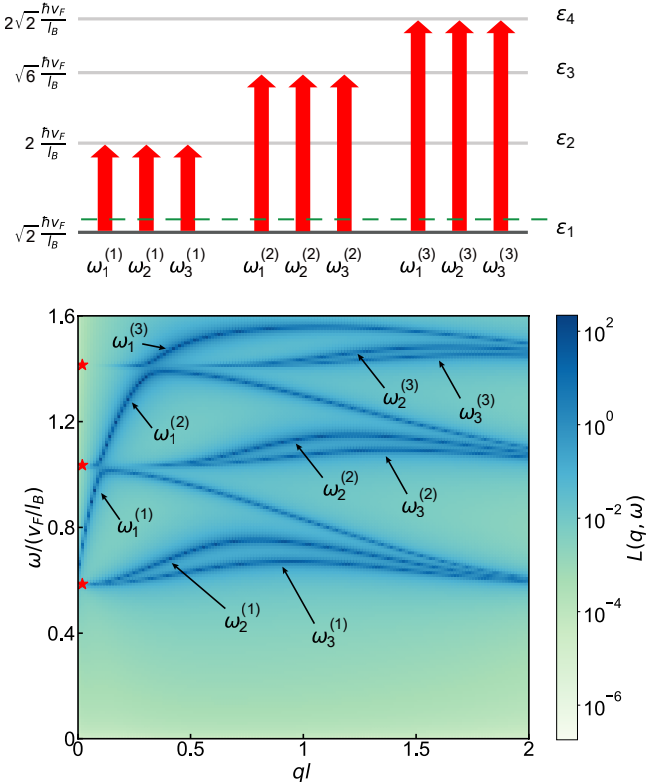


FIG. 7. Schematic illustration of magnetoplasmons associated with each band transition, together with the loss function plot $L(\mathbf{q}, \omega) = -\text{Im} \text{Tr}[\epsilon^{-1}(\mathbf{q}, \omega)]$, for a decoupled trilayer graphene system filled up to the state ϵ_1 . We use the parameters $\kappa = 3.03$, $d = 20 \text{ \AA}$, $\hbar v_F = \frac{\sqrt{3}}{2} \gamma_0 a$, $a = 2.46 \text{ \AA}$, $\gamma_0 = 3.1 \text{ eV}$, $l = 100 \text{ \AA}$, and $\eta = 10^{-3} \hbar\omega_B = 10^{-3} \sqrt{2} \hbar v_F/l$.

level spacing, each dispersion mode $\omega^{(k)}$ in single-layer graphene emerges from the associated inter-Landau-level transitions, analogous to the 2DEG case. Here we label the magnetoplasmon modes with a positive integer k , such that $k = 1$ corresponds to the lowest energy mode, $k = 2$ to the next lowest, and so forth. In a decoupled N -layer graphene system filled up to the state ε_1 , the dispersion $\omega^{(k)}$ splits into $\omega_\alpha^{(k)}$ ($\alpha = 1, \dots, N$) due to the layer degrees of freedom, similar to the decoupled 2DEG multilayer systems illustrated in Fig. 2 (see Fig. 7 for tri-layer graphene results). $\omega_1^{(k)}$ corresponds to one in-phase mode and $\omega_{\alpha \neq 1}^{(k)}$ corresponds to out-of-phase modes.

It is worth noting that, in principle, the hybridization governed by parity and subband-index-reversal symme-

try remains valid in the presence of interlayer tunneling t . This is because the subband wave function is separable from the in-plane Landau level wave function [see Eq. (1)], which allows the selection rules inherent in the Coulomb eigenvector basis to apply in the same manner as in the main text. Similarly, the tunneling magnetoplasmon $\tilde{\omega}_\alpha$ arises from intra-Landau-level transitions, subject to additional Coulomb corrections relative to the underlying interband gap. However, the application of these rules to clarify the dispersion structures in multilayer graphene is often limited due to the complexity arising from the $t \gg \hbar\omega_c$ condition in general multilayer graphene systems [57–59] and from the unequally spaced Landau levels.

-
- [1] A. Y. Cho and J. R. Arthur, Molecular beam epitaxy, *Prog. Solid State Chem.* **10**, 157 (1975).
- [2] K. S. Novoselov, A. K. Geim, S. V. Morozov, D. Jiang, Y. Zhang, S. V. Dubonos, I. V. Grigorieva, and A. A. Firsov, Electric Field Effect in Atomically Thin Carbon Films, *Science* **306**, 666 (2004).
- [3] J. N. Coleman, M. Lotya, A. O'Neill, S. D. Bergin, P. J. King, U. Khan, K. Young, A. Gaucher, S. De, R. J. Smith, I. V. Shvets, S. K. Arora, G. Stanton, H.-Y. Kim, K. Lee, G. T. Kim, G. S. Duesberg, T. Hallam, J. J. Boland, J. J. Wang, J. F. Donegan, J. C. Grunlan, G. Moriarty, A. Shmeliov, R. J. Nicholls, J. M. Perkins, E. M. Grieveson, K. Theuwissen, D. W. McComb, P. D. Nellist, and V. Nicolosi, Two-Dimensional Nanosheets Produced by Liquid Exfoliation of Layered Materials, *Science* **331**, 568 (2011).
- [4] R. Dingle, W. Wiegmann, and C. H. Henry, Quantum States of Confined Carriers in Very Thin $\text{Al}_x\text{Ga}_{1-x}\text{As}-\text{GaAs}-\text{Al}_x\text{Ga}_{1-x}\text{As}$ Heterostructures, *Phys. Rev. Lett.* **33**, 827 (1974).
- [5] B. Radisavljevic, A. Radenovic, J. Brivio, V. Giacometti, and A. Kis, Single-layer MoS₂ transistors, *Nat. Nanotechnol.* **6**, 147 (2011).
- [6] M. Chhowalla, H. S. Shin, G. Eda, L.-J. Li, K. P. Loh, and H. Zhang, The chemistry of two-dimensional layered transition metal dichalcogenide nanosheets, *Nat. Chem.* **5**, 263 (2013).
- [7] Y.-C. Lin, B. Jariwala, B. M. Bersch, K. Xu, S. M. Eichfeld, X. Zhang, T. H. Choudhury, Y. Pan, R. Addou, C. M. Smyth, J. Li, K. Zhang, M. A. Haque, S. Fölsch, R. M. Feenstra, R. M. Wallace, K. Cho, S. K. Fullerton-Shirey, J. M. Redwing, and J. A. Robinson, Realizing Large-Scale, Electronic-Grade Two-Dimensional Semiconductors, *ACS Nano* **12**, 965 (2018).
- [8] C. X. Trang, Q. Li, Y. Yin, J. Hwang, G. Akhgar, I. D. Bernardo, A. Grubišić-Cabo, A. Tadich, M. S. Fuhrer, S.-K. Mo, N. V. Medhekar, and M. T. Edmonds, Crossover from 2D Ferromagnetic Insulator to Wide Band Gap Quantum Anomalous Hall Insulator in Ultrathin MnBi₂Te₄, *ACS Nano* **15**, 13444 (2021).
- [9] Y. Lei, T. Zhang, Y.-C. Lin, T. Granzier-Nakajima, G. Bepete, D. A. Kowalczyk, Z. Lin, D. Zhou, T. F. Schranghamer, A. Dodda, A. Sebastian, Y. Chen, Y. Liu, G. Pourtois, T. J. Kempa, B. Schuler, M. T. Edmonds, S. Y. Quek, U. Wurstbauer, S. M. Wu, N. R. Glavin, S. Das, S. P. Dash, J. M. Redwing, J. A. Robinson, and M. Terrones, Graphene and Beyond: Recent Advances in Two-Dimensional Materials Synthesis, Properties, and Devices, *ACS Nanosci. Au* **2**, 450 (2022).
- [10] R. E. V. Profumo, M. Polini, R. Asgari, R. Fazio, and A. H. MacDonald, Electron-electron interactions in decoupled graphene layers, *Phys. Rev. B* **82**, 085443 (2010).
- [11] Y. Jang, E. H. Hwang, A. H. MacDonald, and H. Min, Stacking dependence of carrier interactions in multilayer graphene systems, *Phys. Rev. B* **92**, 041411 (2015).
- [12] K. Liu, L. Zhang, T. Cao, C. Jin, D. Qiu, Q. Zhou, A. Zettl, P. Yang, S. G. Louie, and F. Wang, Evolution of interlayer coupling in twisted molybdenum disulfide bilayers, *Nat. Commun.* **5**, 4966 (2014).
- [13] K. Shin, Y. Jang, J. Shin, J. Jung, and H. Min, Electronic structure of biased alternating-twist multilayer graphene, *Phys. Rev. B* **107**, 245139 (2023).
- [14] R. V. Gorbachev, A. K. Geim, M. I. Katsnelson, K. S. Novoselov, T. Tudorovskiy, I. V. Grigorieva, A. H. MacDonald, S. V. Morozov, K. Watanabe, T. Taniguchi, and L. A. Ponomarenko, Strong Coulomb drag and broken symmetry in double-layer graphene, *Nat. Phys.* **8**, 896 (2012).
- [15] G. W. Burg, N. Prasad, B. Fallahazad, A. Valsaraj, K. Kim, T. Taniguchi, K. Watanabe, Q. Wang, M. J. Kim, L. F. Register, and E. Tutuc, Coherent Interlayer Tunneling and Negative Differential Resistance with High Current Density in Double Bilayer Graphene–WSe₂ Heterostructures, *Nano Lett.* **17**, 3919 (2017).
- [16] P. V. Nguyen, N. C. Teutsch, N. P. Wilson, J. Kahn, X. Xia, A. J. Graham, V. Kandyba, A. Giampietri, A. Barinov, G. C. Constantinescu, N. Yeung, N. D. M. Hine, X. Xu, D. H. Cobden, and N. R. Wilson, Visualizing electrostatic gating effects in two-dimensional heterostructures, *Nature* **572**, 220 (2019).
- [17] S. Kim, I. Jo, J. Nah, Z. Yao, S. K. Banerjee, and E. Tutuc, Coulomb drag of massless fermions in graphene, *Phys. Rev. B* **83**, 161401 (2011).
- [18] J. C. W. Song and L. S. Levitov, Energy-Driven Drag at Charge Neutrality in Graphene, *Phys. Rev. Lett.* **109**, 236602 (2012).

- [19] L. Wang, E.-M. Shih, A. Ghiotto, L. Xian, D. A. Rhodes, C. Tan, M. Claassen, D. M. Kennes, Y. Bai, B. Kim, K. Watanabe, T. Taniguchi, X. Zhu, J. Hone, A. Rubio, A. N. Pasupathy, and C. R. Dean, Correlated electronic phases in twisted bilayer transition metal dichalcogenides, *Nat. Mater.* **19**, 861 (2020).
- [20] Y. Cao, V. Fatemi, S. Fang, K. Watanabe, T. Taniguchi, E. Kaxiras, and P. Jarillo-Herrero, Unconventional superconductivity in magic-angle graphene superlattices, *Nature* **556**, 43 (2018).
- [21] J. I. A. Li, T. Taniguchi, K. Watanabe, J. Hone, and C. R. Dean, Excitonic superfluid phase in double bilayer graphene, *Nat. Phys.* **13**, 751 (2017).
- [22] X. Liu, K. Watanabe, T. Taniguchi, B. I. Halperin, and P. Kim, Quantum Hall drag of exciton condensate in graphene, *Nat. Phys.* **13**, 746 (2017).
- [23] Z. Wang, D. A. Rhodes, K. Watanabe, T. Taniguchi, J. C. Hone, J. Shan, and K. F. Mak, Evidence of high-temperature exciton condensation in two-dimensional atomic double layers, *Nature* **574**, 76 (2019).
- [24] F. Stern, Polarizability of a Two-Dimensional Electron Gas, *Phys. Rev. Lett.* **18**, 546 (1967).
- [25] S. J. Allen, D. C. Tsui, and R. A. Logan, Observation of the Two-Dimensional Plasmon in Silicon Inversion Layers, *Phys. Rev. Lett.* **38**, 980 (1977).
- [26] E. H. Hwang and S. Das Sarma, Dielectric function, screening, and plasmons in two-dimensional graphene, *Phys. Rev. B* **75**, 205418 (2007).
- [27] Z. Fei, A. S. Rodin, G. O. Andreev, W. Bao, A. S. McLeod, M. Wagner, L. M. Zhang, Z. Zhao, M. Thiemens, G. Dominguez, M. M. Fogler, A. H. Castro Neto, C. N. Lau, F. Keilmann, and D. N. Basov, Gate-tuning of graphene plasmons revealed by infrared nano-imaging, *Nature* **487**, 82 (2012).
- [28] A. N. Grigorenko, M. Polini, and K. S. Novoselov, Graphene plasmonics, *Nat. Photonics* **6**, 749 (2012).
- [29] J. Chen, M. Badioli, P. Alonso-González, S. Thongrattanasiri, F. Huth, J. Osmond, M. Spasenović, A. Centeno, A. Pesquera, P. Godignon, A. Zurutuza Elorza, N. Camara, F. J. G. de Abajo, R. Hillenbrand, and F. H. L. Koppens, Optical nano-imaging of gate-tunable graphene plasmons, *Nature* **487**, 77 (2012).
- [30] Z. Fei, E. G. Iwinski, G. X. Ni, L. M. Zhang, W. Bao, A. S. Rodin, Y. Lee, M. Wagner, M. K. Liu, S. Dai, M. D. Goldflam, M. Thiemens, F. Keilmann, C. N. Lau, A. H. Castro-Neto, M. M. Fogler, and D. N. Basov, Tunneling Plasmonics in Bilayer Graphene, *Nano Lett.* **15**, 4973 (2015).
- [31] P. Novelli, I. Torre, F. H. L. Koppens, F. Taddei, and M. Polini, Optical and plasmonic properties of twisted bilayer graphene: Impact of interlayer tunneling asymmetry and ground-state charge inhomogeneity, *Phys. Rev. B* **102**, 125403 (2020).
- [32] I. B. Bernstein, Waves in a Plasma in a Magnetic Field, *Phys. Rev.* **109**, 10 (1958).
- [33] K. W. Chiu and J. J. Quinn, Plasma oscillations of a two-dimensional electron gas in a strong magnetic field, *Phys. Rev. B* **9**, 4724 (1974).
- [34] S. Das Sarma and J. J. Quinn, Collective excitations in semiconductor superlattices, *Phys. Rev. B* **25**, 7603 (1982).
- [35] C. Kallin and B. I. Halperin, Excitations from a filled Landau level in the two-dimensional electron gas, *Phys. Rev. B* **30**, 5655 (1984).
- [36] V. Bonanni, S. Bonetti, T. Pakizeh, Z. Pirzadeh, J. Chen, J. Nogués, P. Vavassori, R. Hillenbrand, J. Åkerman, and A. Dmitriev, Designer Magnetoplasmonics with Nickel Nanoferromagnets, *Nano Lett.* **11**, 5333 (2011).
- [37] E. Melander, E. Östman, J. Keller, J. Schmidt, E. T. Papaioannou, V. Kapaklis, U. B. Arnalds, B. Sanyal, A. Dmitriev, and B. Hjörvarsson, Influence of the magnetic field on the plasmonic properties of transparent Ni anti-dot arrays, *Appl. Phys. Lett.* **101**, 063107 (2012).
- [38] F. Pineider, G. Campo, V. Bonanni, C. de Julián Fernández, G. Mattei, A. Caneschi, D. Gatteschi, and C. Sangregorio, Circular Magnetoplasmonic Modes in Gold Nanoparticles, *Nano Lett.* **13**, 4785 (2013).
- [39] G. Armelles, A. Cebollada, A. García-Martín, and M. U. González, Magnetoplasmonics: Combining Magnetic and Plasmonic Functionalities, *Adv. Optical Mater.* **1**, 10 (2013).
- [40] B. Han, X. Gao, L. Shi, Y. Zheng, K. Hou, J. Lv, J. Guo, W. Zhang, and Z. Tang, Geometry-Modulated Magnetoplasmonic Optical Activity of Au Nanorod-Based Nanostructures, *Nano Lett.* **17**, 6083 (2017).
- [41] N. Maccaferri, K. E. Gregorczyk, T. V. A. G. de Oliveira, M. Kataja, S. van Dijken, Z. Pirzadeh, A. Dmitriev, J. Åkerman, M. Knez, and P. Vavassori, Ultrasensitive and label-free molecular-level detection enabled by light phase control in magnetoplasmonic nanoantennas, *Nat. Commun.* **6**, 6150 (2015).
- [42] Q. Zhang, M. Lou, X. Li, J. L. Reno, W. Pan, J. D. Watson, M. J. Manfra, and J. Kono, Collective non-perturbative coupling of 2D electrons with high-quality-factor terahertz cavity photons, *Nat. Phys.* **12**, 1005 (2016).
- [43] J. Keller, G. Scalari, S. Cibella, C. Maissen, F. Appugliese, E. Giovine, R. Leoni, M. Beck, and J. Faist, Few-electron ultrastrong light-matter coupling at 300 GHz with nanogap hybrid LC microcavities, *Nano Letters* **17**, 7410 (2017).
- [44] I. Grigelionis, K. Nogajewski, G. Karczewski, T. Wojtowicz, M. Czapkiewicz, J. Wróbel, H. Boukari, H. Mariette, and J. Lusakowski, Magnetoplasmons in high electron mobility CdTe/CdMgTe quantum wells, *Phys. Rev. B* **91**, 075424 (2015).
- [45] M. B. Lundeberg, Y. Gao, R. Asgari, C. Tan, B. Van Duppen, M. Autore, P. Alonso-González, A. Woessner, K. Watanabe, T. Taniguchi, R. Hillenbrand, J. Hone, M. Polini, and F. H. L. Koppens, Tuning quantum nonlocal effects in graphene plasmonics, *Science* **357**, 187 (2017).
- [46] L. Cao, Q. Fu, B. Wu, and Y. Xiong, Terahertz magnetoplasmon-polaritons with nonlocal corrections for lossy two dimensional electron gas in GaN-based heterostructures, *Journal of Physics: Condensed Matter* **29**, 395302 (2017).
- [47] G. R. Ažin and G. Gumbs, Tunneling magnetoplasmon excitations in the semiclassical limit and integer quantum Hall regime for double-quantum-well systems, *Phys. Rev. B* **52**, 1890 (1995).
- [48] G. Mahan, *Many-Particle Physics* (Springer US, 1990).
- [49] G. F. Giuliani and G. Vignale, *Quantum Theory of the Electron Liquid* (Cambridge University Press, 2005).
- [50] R. Roldán, J.-N. Fuchs, and M. O. Goerbig, Collective modes of doped graphene and a standard two-

- dimensional electron gas in a strong magnetic field: Linear magnetoplasmons versus magnetoexcitons, *Phys. Rev. B* **80**, 085408 (2009).
- [51] T. Kim, E. H. Hwang, and H. Min, Plasmons in N -layer systems, *Phys. Rev. B* **112**, L041111 (2025).
- [52] G. S. M. Kac, W. Murdock, On the Eigen-Values of Certain Hermitian Forms, *Indiana Univ. Math. J.* **2**, 767 (1953).
- [53] W. F. Trench, Properties of Some Generalizations of Kac–Murdock–Szegő Matrices, *Contemp. Math.* **281**, 233 (2001).
- [54] J. M. Bogoya, A. Böttcher, S. M. Grudsky, and E. A. Maximenko, Eigenvectors of Hermitian Toeplitz matrices with smooth simple-loop symbols, *Linear Algebra Appl.* **493**, 606 (2016).
- [55] G. Fikioris, Spectral properties of Kac–Murdock–Szegő matrices with a complex parameter, *Linear Algebra Appl.* **553**, 182 (2018).
- [56] O. Narayan and B. S. Shastry, Generalized Toeplitz–Hankel matrices and their application to a layered electron gas, *J. Phys. A: Math. Theor.* **54**, 175201 (2021).
- [57] M. Tahir and K. Sabeeh, Inter-band magnetoplasmons in mono- and bilayer graphene, *J. Phys.: Condens. Matter* **20**, 425202 (2008).
- [58] O. L. Berman, G. Gumbs, and Y. E. Lozovik, Magnetoplasmons in layered graphene structures, *Phys. Rev. B* **78**, 085401 (2008).
- [59] A. H. Castro Neto, F. Guinea, N. M. R. Peres, K. S. Novoselov, and A. K. Geim, The electronic properties of graphene, *Rev. Mod. Phys.* **81**, 109 (2009).